Int. J. Electrochem. Sci., 14 **(2019)** 5408 – 5421, doi: 10.20964/2019.06.67

International Journal of
ELECTROCHEMICAL
SCIENCE
www.electrochemsci.org

Roughened Graphite Felt Electrode with Enhanced Electrochemical Activity for Vanadium Redox Flow Batteries

Lei Chen, Haixia Zhou, Youqun Chu[*]*, Shaoping Tong*

State Key Laboratory Breeding Base of Green Chemistry-Synthesis Technology,
Chemical Engineering College, Zhejiang University of Technology, Hangzhou 310014, China
[*]E-mail: chuyq@zjut.edu.cn

Received: 2 March 2019 / *Accepted:* 9 April 2019 / *Published:* 10 May 2019

A simple and effective method to roughen graphite felt (GF) by using manganese oxide as an etching agent has been developed for vanadium redox flow battery (VRFB) application. The specific surface area of roughened GF (R-GF) prepared at the optimized conditions reaches 8.49 $m^2 \cdot g^{-1}$, 7 times larger than that of the pristine one (P-GF), and more oxygen-containing functional groups are formed on the roughened surface. The experimental results show that the R-GF has higher peak current, smaller peak potential separation and lower charge transfer resistance than those of P-GF and GF treated with air oxidation (O-GF). The VRFB with R-GF electrodes exhibits a strongly enhanced electrochemical performance in terms of energy efficiency and utilization ratio of electrolyte at different current density. The large specific surface area with abundant oxygen-containing functional groups of R-GF has been shown to be extremely beneficial for improving the kinetics of the VRFB.

Keywords: vanadium redox flow battery, etching, roughened graphite felt, electrochemical activity.

1. INTRODUCTION

With the rapid development of renewable energy sources such as wind energy and solar power, an effective large-scale energy storage system is urgently needed to overcome their intermittent and instable nature [1, 2]. Among all the new energy storage technologies currently under development, vanadium redox flow battery (VRFB) is one of the most promising candidates suitable for industrial and utility-scale applications. VRFB employs four different vanadium ions, VO^{2+}/VO_2^+ redox couple in positive electrolyte and V^{2+}/V^{3+} redox couple in negative electrolyte, which are stored in two isolated reservoirs [3-6]. Compared with other batteries, the energy of VRFB depends on the concentration of vanadium species and the volume of electrolyte in the reservoir, while the system power is determined by the reaction kinetics of vanadium species at each electrode and the total electrode surface area.

Graphite felt (GF) has been typically used as the electrode material for VRFB, attributed to its low cost, good electrical conductivity, high mechanical and chemical stability. However, the poor electrochemical activity of pristine GF (P-GF) for the redox reactions of vanadium species limits the performance of VRFB. In this regard, many efforts have been made to modify the GF surface by introducing O- or N-containing functional groups through acid treatment [7], chemical or electrochemical oxidation [8], thermal treatment [9], as well as adding carbon-based or metal-based materials as electrocatalysts (e.g. carbon nanotubes, graphene, Bi, Pt, Cu, WO_3, ZrO_2, Nb_2O_5, TiN) [10-19], which effectively enhance the electrochemical reaction kinetics of vanadium species on GF. However, the modified electrodes are seldom used in VRFB practically so far, which can be ascribed to the poor stability of electrode performance resulting from the degradation of O- or N-containing functional groups during repeated charge/discharge cycling and the supported electrocatalyst particles shedding by the flowing electrolyte.

Besides the surface electrochemical activity, specific surface area of electrode is another critical parameter for the electrochemical systems. Unfortunately, the specific surface areas of commonly used P-GFs are fairly small (about 1 $m^2 \cdot g^{-1}$) [20], which inevitably leads to higher electrochemical polarization and thereby limits the VRFB performance. To break through this barrier, many researchers have attempted to increase the specific surface area through roughening the GF fibers by various etching methods, such as CO_2 etching [21], water vapor etching [22], KOH etching [23], NiO etching [24], FeOOH etching [25], and Co_3O_4 etching [26]. Under these efforts, increased specific surface areas (5-20 $m^2 \cdot g^{-1}$) and better overall VRFB performances have been reported. These results demonstrate the effectiveness to improve VRFB performance by increasing the specific surface area of GF. However, the above-mentioned etching processes are carried out under relatively harsh conditions, such as high temperature, inert atmosphere, or using expensive metal oxides, which limit the practical application of these methods. Therefore, there is still a pressing need to develop various methods to roughening the GF fibers to increase the surface area.

Here, we report a simple and cost-effective method to increase the GF surface area using cheap manganese oxide as etching agent. The roughness of GF fibers can be easily controlled by varying the concentration of precursor solution and the temperature of etching process. The roughened GF (R-GF) prepared under optimized conditions shows a specific surface area of 8.49 $m^2 \cdot g^{-1}$, which is 7 times larger than that of P-GF (1.18 $m^2 \cdot g^{-1}$). In addition, the surface of R-GF contains substantial oxygen-containing functional groups with high wettability, which could provide more active sites for the redox reaction of vanadium ions and reduce concentration polarization [27]. The VRFB with R-GF electrodes shows significantly enhanced electrochemical performance and stability during charge/discharge cycling when compared with those with other GF electrodes.

2. EXPERIMENTAL

2.1. Materials

Poly(acrylonitrile) based GF (5 mm of thickness, Haoshi Carbon Fiber) was employed as electrode substrate. Manganese acetate tetrahydrate ($Mn(CH_3COO)_2 \cdot 4H_2O$, 99 %, Aladdin) was used

as metal oxide precursor. The electrolyte solution was prepared by dissolving an appropriate amount of vanadium sulfate hydrated ($VOSO_4 \cdot 4H_2O$, 99 %, Sinopharm chemical), and sulfuric acid (H_2SO_4, 99 %, Sinopharm chemical). Nafion 115 membrane was purchased from DuPont Company and treated by standard acid boiling procedure before use [28]. All reagents were of analytical grade and used directly without further purification.

2.2. Preparation of roughened graphite felts

P-GFs were treated in ethanol, acetone and deionized water successively in the ultrasonic bath to remove impurities, then thermally treated at 500 °C in an air atmosphere for 2 h to obtain the oxidized GFs (O-GFs). After cooling, the O-GFs were immersed in the precursor solution of 0.005-0.08 M manganese acetate tetrahydrate and sonicated for 2 h, then dried overnight in a vacuum oven. Finally, the precursor layer was uniformly coated on the GFs. The precursor coated GFs were thermal treatment at 200 °C for 1 h in air to form Mn_3O_4 coated GFs. After that, the temperature was further raised to 300-600 °C and retained for 2 h to etch GF fibers. The resulting Mn_3O_4 decorated R-GFs (D-GFs) were washed with 1 M HNO_3, 3 M HCl and deionized water in turn to eliminate the residuals. Finally, the R-GFs were obtained after drying.

2.3. Characterization

The surface morphologies of GFs were characterized by scanning electron microscopy (SEM, FEI Nova Nano 450) at the acceleration voltage of 15 kV. The compositions of GFs were investigated by X-ray diffraction (XRD, Panalytical, X'Pert Pro). The X-ray photoelectron spectroscopy (XPS, Sigma Probe, Thermo VG Scientific) was used to examine the surface chemistry. The Brunauer-Emmett-Teller (BET) specific surface area was measured by N_2 adsorption analyzer (Micromeritics ASAP2020).

2.4. Electrochemical measurements

To investigate the electrochemical properties of the GF electrodes, cyclic voltammetry (CV) and electrochemical impedance spectroscopy (EIS) measurements were carried out in a typical three-electrode system using an electrochemical workstation (IviumStat) at room temperature. A saturated calomel electrode (SCE) and a platinum plate were used as the reference and counter electrodes, respectively. A piece of GF with a geometric area of 1 cm^2 was used as the working electrode. CV measurements were conducted in 0.1 M $VOSO_4$ /2 M H_2SO_4 solution in the potential range of 0.2 V to 1.5 V and in 0.1 M $V_2(SO_4)_3$/2 M H_2SO_4 solution in potential range of -0.8 V to -0.2 V, respectively. EIS measurements were carried out at 0.9 V in 0.1 M $VOSO_4$/2 M H_2SO_4 solution and -0.4 V in 0.1 M $V_2(SO_4)_3$/2 M H_2SO_4 solution in the frequency range of 100 kHz to 10 mHz.

2.5. Evaluation of a VRFB single cell

A VRFB single cell was fabricated by sandwiching a piece of Nafion 115 (8 cm×8 cm) membrane between two pieces of 3 cm×3 cm GFs. 20 mL 1.5 M $VOSO_4$ in 3 M H_2SO_4 solution and 20 mL 1.5 M $V_2(SO_4)_3$ in 3 M H_2SO_4 solution serving as positive and negative electrolytes were circulated through the cell at a flow rate of 10 $mL \cdot min^{-1}$ by using BT100-1L peristaltic pumps (Baoding Longer). The performance of VRFBs was evaluated at room temperature on a CT2001A battery test system (Wuhan Lanhe) within the cell voltage range of 0.8-1.65 V.

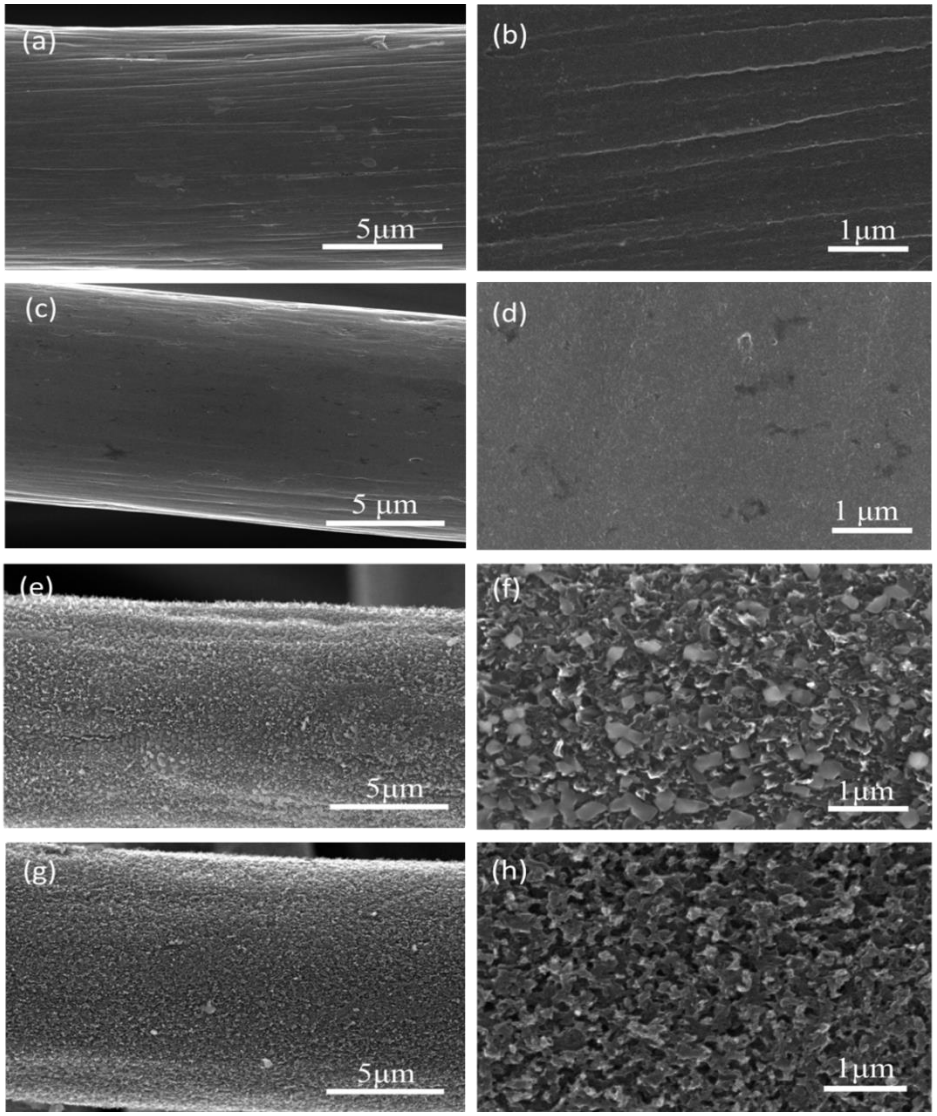

Figure 1. Low- and high-magnification SEM images of (a, b) P-GF; (c, d) O-GF; (e, f) Mn_3O_4 decorated GF and (g, h) R-GF, showing the surface morphology of the fibers comprising the electrodes.

3. RESULTS AND DISCUSSION

The morphologies of different GF fibers are shown in Fig.1. Compared with P-GF (Fig.1a, b), O-GF has a smoother surface **(**Fig.1c, d), which can be ascribed to the oxidative decomposition of

surface defects and impurities of P-GF during the thermal treating process. However, the roughened surface morphology can be observed from Fig.1e and f when the manganese oxide coated GFs are heat treated under the similar conditions as O-GF. This certifies that the manganese oxide can be used as an etching agent as NiO [24], FeOOH [25] and Co_3O_4 [26] to roughen the GF fibers. The XRD patterns of D-GFs (Fig. 2a, b) confirm the manganese oxide is Mn_3O_4 (JCPDS#24-0734). Based on the redox reaction of the manganese oxide [29, 30], an etching mechanism similar to the above-mentioned literatures [24-26] can be deduced: The Mn_3O_4 acts as an oxidative reagent which reacts with the carbon to form MnO, and then the resulting MnO is oxidized by air to form Mn_3O_4 again. The repeated occurrence of Mn_3O_4/MnO redox reactions results in the roughened surface morphology of D-GFs, and the preparation process of R-GF can be schematically expressed in Fig. 3.

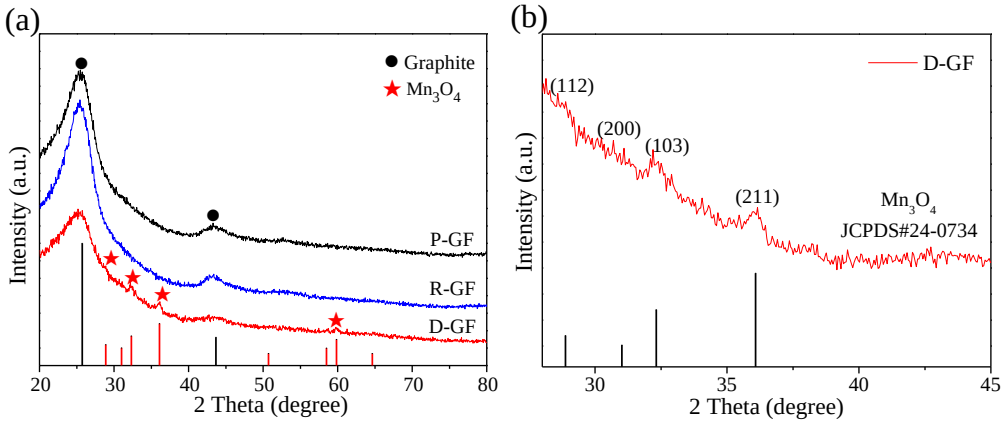

Figure 2. (a) XRD patterns of the P-GF, D-GF and R-GF samples. (b) XRD pattern of D-GF in magnified portion.

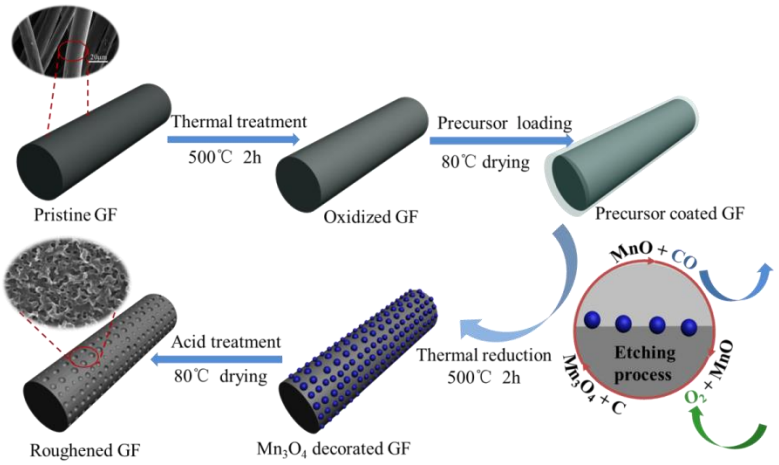

Figure 3. Schematic of the fabrication process of roughened graphite felt.

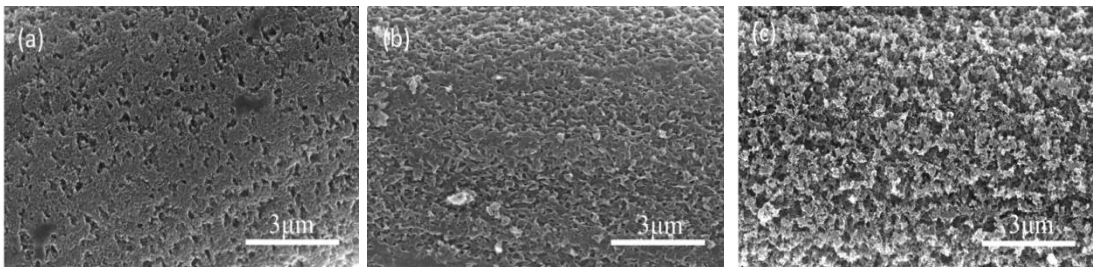

Figure 4. SEM images of the R-GF surface morphology after acid treatment at the precursor concentrations of (a) 0.005 M, (b) 0.02 M, and (c) 0.08 M.

According to the above etching mechanism, the roughness of etched GFs is determined by several parameters, such as the precursor concentration and the operating temperature of Mn_3O_4 reduction reaction. Fig. 4 shows the effects of precursor concentration (0.005, 0.02 and 0.08 M) on the morphologies of R-GFs. The GFs are sparsely etched at lower concentration (0.005 M) while excessively etched at higher concentration (0.08 M). In addition, the effect of operating temperature is also investigated in the range of 300-600 °C with the precursor concentration of 0.02 M. As shown in Fig. 5, a few etched pits can be observed on the R-GF prepared at 300 °C, and the roughness increases with the temperature. When the temperature reaches 600 °C, the surface of GF fiber is seriously damaged. Based on the above results, a precursor concentration of 0.02 M and an operating temperature of 500 °C are considered as the optimized the parameters to obtain highly roughened GFs without causing serious damage to the fiber structure.

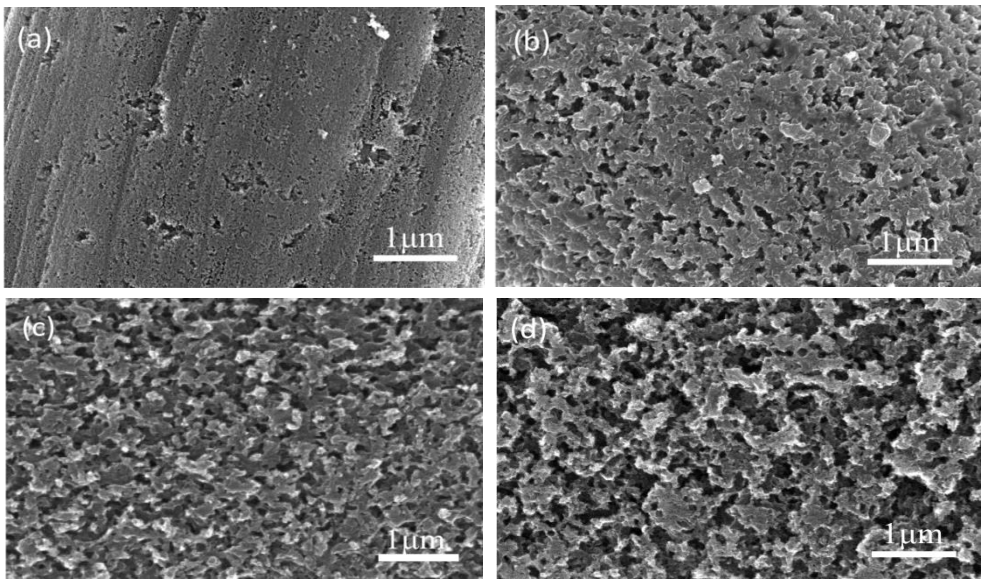

Figure 5. SEM images of the R-GF surface morphology after acid treatment at annealing temperatures of (a) 300 °C, (b) 400 °C, (c) 500 °C and (d) 600 °C with 0.02 M precursor solution.

In order to further compare the physical and electrochemical properties, P-GF and O-GF were selected as the comparative objects. The BET specific surface area of R-GF prepared under the optimized condition is 8.49 $m^2 \cdot g^{-1}$, considerably larger than those of P-GF (1.18 $m^2 \cdot g^{-1}$) and O-GF (2.79 $m^2 \cdot g^{-1}$). It is also proved that the roughening of GF is successfully achieved by using Mn_3O_4 as

the etching agent. The increase of specific surface area of R-GF is expected to benefit the vanadium redox reactions. In addition to the specific surface area, the surface properties are also crucial to the performance of electrode. Thus, the XPS characterization is carried out, shown in Fig. 6 and Table 1. As the results reported in the literatures [8, 9], oxygen-containing functional groups can be introduced onto the surface of GF after heat treatment in an air atmosphere (Fig.6a). The content of oxygen-containing functional groups of O-GF increases by more than 4 times, from 1.99 % of P-GF to 8.72 % of O-GF. R-GF shows the similar XPS spectra as that of O-GF, while the highest content of oxygen-containing functional groups on R-GF (11.77 %) is detected.

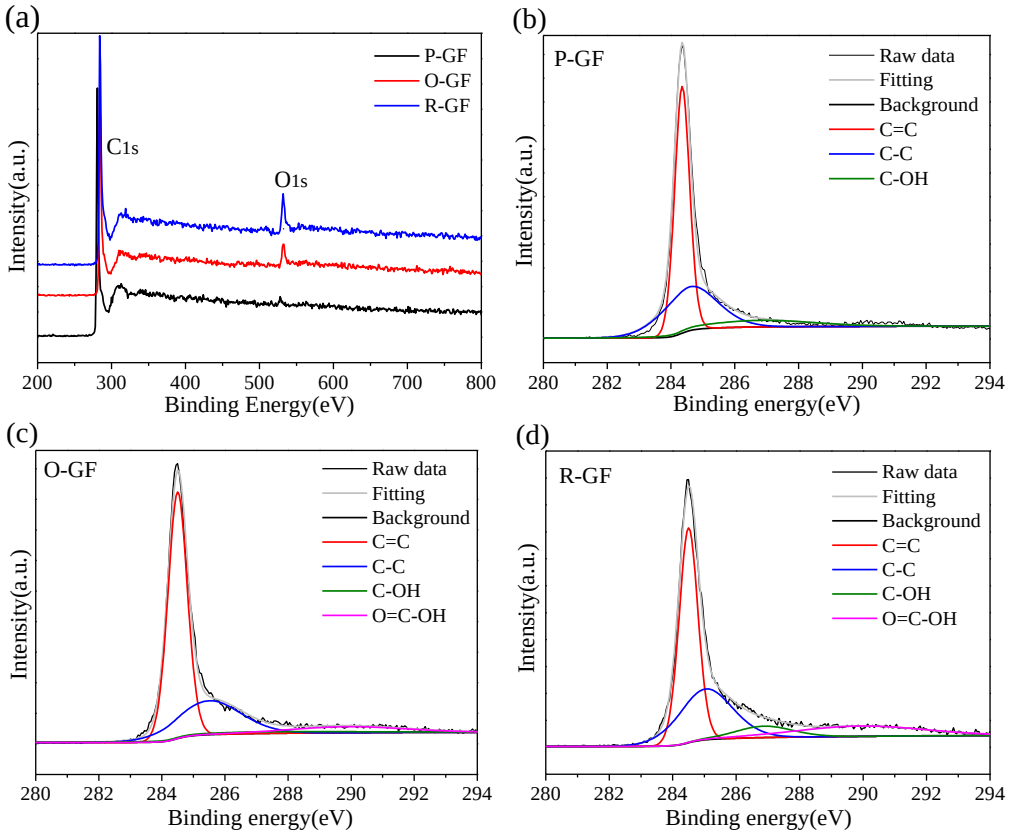

Figure 6. (a) XPS survey spectra in wide-range scan, XPS C1s spectra of (b) P-GF, (c) O-GF, and (d) R-GF.

This can be ascribed to the larger specific surface area of R-GF, which is conducive to the formation of oxygen-containing functional groups. As shown in Fig.6b-d, the C1s spectra of all GFs can be deconvoluted into three or four peaks at the binding energy of 284.5, 285.3, 286.8 and 288.9 eV, corresponding to C=C, C-C, C-OH and COOH functional groups, respectively [21,22]. The R-GF has the highest contents of COOH (4.70%) and C-OH (7.07%) groups. This increase results from the massive oxygen defects formed on the R-GF during the etching process, which not only enhances the hydrophilicity of R-GFs, but also provides more active sites for vanadium redox reactions [31]. R-GFs with larger hydrophilic surface area and more active centers could be favorable to enhance the efficiency of the VRFB system.

Table 1. Chemical composition ratio of functional groups from curve fitting of C1s.

Samples	C 1s (%)	O 1s (%)	C=C (%)	C-C (%)	C-OH (%)	COOH (%)
P-GF	98.01	1.99	59.57	38.44	1.99	—
O-GF	91.28	8.72	54.19	27.08	6.47	3.54
R-GF	88.23	11.77	50.98	25.48	7.07	4.70

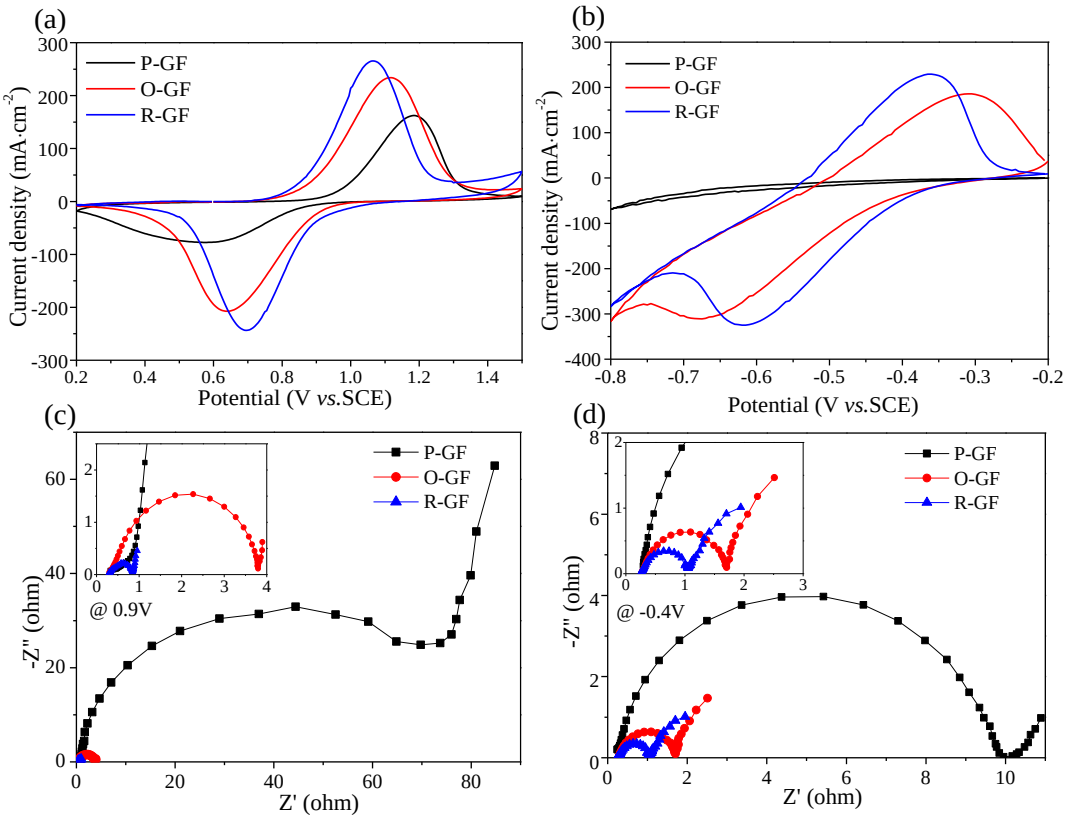

Figure 7. CV curves of P-GF, O-GF and R-GF at a scan rate of 10 mV·s^{-1} in (a) positive electrolyte and (b) negative electrolyte. Nyquist plots of P-GF, O-GF and R-GF in (c) positive reaction and (d) negative reaction.

Fig. 7a and b present the CV curves of different GF electrodes in positive and negative electrolytes of VRFBs at a scan rate of 10 mV·s^{-1}. For the P-GF, there is a large peak potential separation of 610 mV for VO^{2+}/VO_2^+ redox reaction, and no obvious peak observed for V^{2+}/V^{3+} redox reaction, which indicates that P-GF has poor electrochemical activity for the redox reactions of vanadium ions. The O-GF has the peak potential separations of 475 and 365 mV in the positive and negative electrolytes, respectively. From the above results, it is confirmed that the introduction of oxygen-containing functional groups onto GF surface is beneficial to reduce polarization of the vanadium redox reaction. Just as expected, the smallest peak potential separations, 370 mV in the positive electrolyte and 260 mV in the negative electrolyte, are obtained on the R-GF electrode. This suggests that the R-GF has the best electrochemical activity compared with P-GF and O-GF, which

can be attributed to its larger surface area with abundant oxygen-containing functional groups as catalytic centers. To further investigate the electrochemical activities of different GFs, the EIS measurements are conducted at the formal potentials (0.9 V for VO^{2+}/VO_2^+ and -0.4 V for V^{2+}/V^{3+}). As shown in Fig. 7c and d, each EIS plot consists of a semicircle part in the high-frequency region and a linear part in the low-frequency region. The diameter of the semicircle reflects the charge transfer resistance (R_{ct}), with a smaller diameter indicating a lower charge transfer resistance, which in turn demonstrates a faster electron transfer reaction. The high frequency intercept of the semicircle on the real axis is the bulk solution resistance (R_s) [32]. The R_s values of all electrodes are nearly equal, which indicates that all samples are properly measured under the same conditions. As for the positive reaction, the R_{ct} value for the R-GF is 0.59 Ω, which is much lower than that for P-GF (93.9 Ω) and O-GF (3.65 Ω). As for the negative reaction, the R_{ct} value for the R-GF (0.82 Ω) is also the smallest. The above results illustrate that the R-GF has excellent electrocatalytic activity towards vanadium redox reactions, which agrees well with the CV tests.

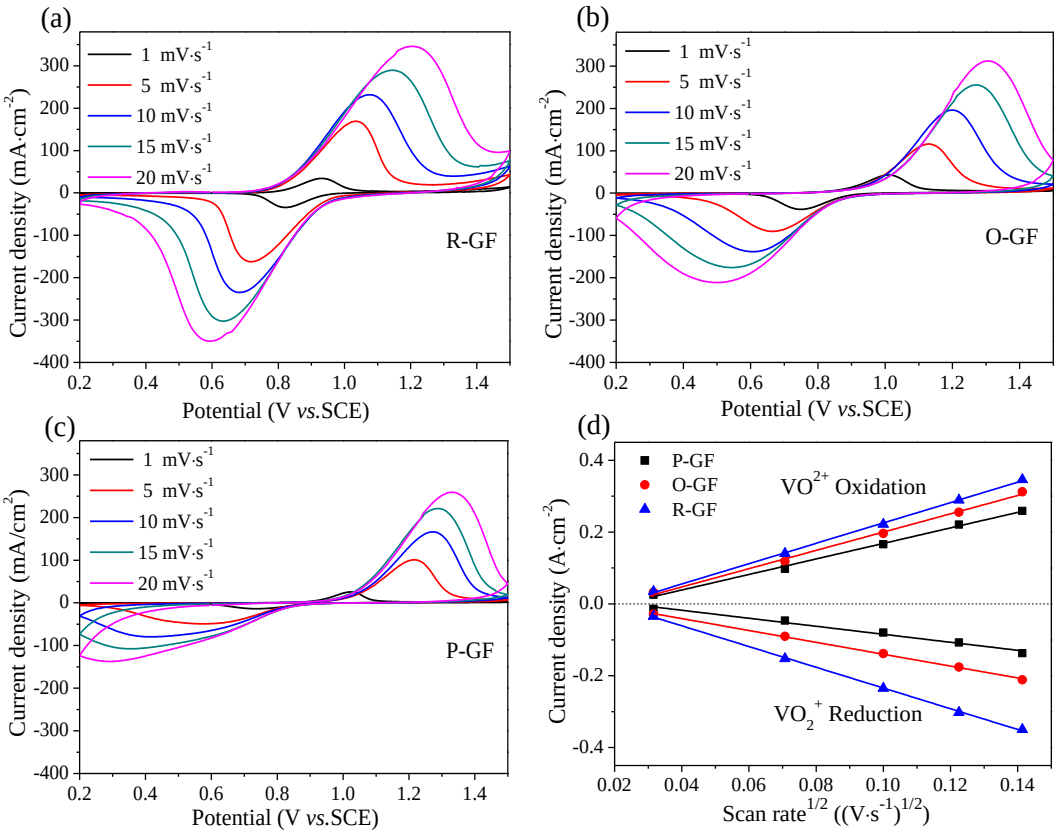

Figure 8. CV curves of (a) R-GF, (b) O-GF, and (c) P-GF at various scan rates. (d) Plots of peak current density versus the square root of the scan rate for the VO^{2+}/VO_2^+ redox reaction.

In addition, the mass transfer properties of the redox reaction of VO^{2+}/VO_2^+ couple on different GFs are also investigated by varying the scan rate of CVs from 1 to 20 $mV \cdot s^{-1}$. As shown in Fig. 8, the peak current density linearly increases with the square root of the scan rate on all GF electrodes, which indicates that the electrode reactions are all controlled by the diffusion step and seldom affected by the surface roughness and surface chemical properties of GFs. The R-GF electrode exhibits higher peak

current densities and smaller peak potential separations than other electrodes at all scan rates, implying the improved electrochemical kinetics for the redox reaction of VO^{2+}/VO_2^+ couple.

In order to verify the effect of R-GF on the performance of VRFB, single cells employing different GF electrodes were undergone charging and discharging cycles at a current density of 80 $mA \cdot cm^{-2}$. Fig. 9a shows the typical discharge profiles of cells with different GF electrodes at the 5th cycle, and the lowest charge voltage and the highest discharge voltage can be observed for the cell using R-GF electrode owing to its improved electrolyte accessibility and reduced electrochemical polarization. Furthermore, the available discharge capacity of R-GF (34.4 $Ah \cdot L^{-1}$) is about 9.6 % and 19.4 % higher than that of O-GF (31.4 $Ah \cdot L^{-1}$) and P-GF (28.8 $Ah \cdot L^{-1}$), respectively. Since the cost of vanadium electrolyte has recently multiplied, more efficiently utilization of the electrolyte is critical to reduce the cost of VRFB system. Fig. 9b shows coulombic efficiency (CE), voltage efficiency (VE) of the batteries. The CEs of all electrodes almost keep the same with the values of 94.0 % owing to the same electrolyte and membrane used.

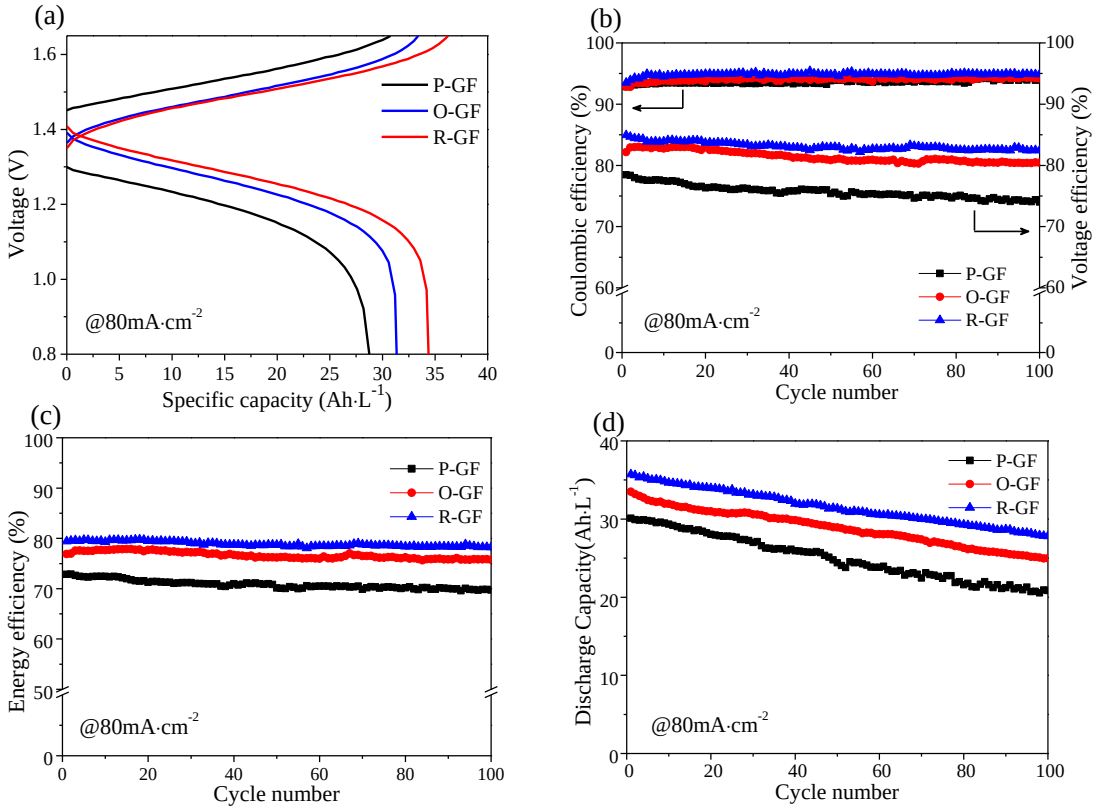

Figure 9. Electrochemical cycling performance of VRFBs using P-GF, O-GF and R-GF electrodes at the current density of 80 $mA \cdot cm^{-2}$: (a) Charge/discharge voltage profiles, (b) Coulombic and voltage efficiency, (c) Energy efficiency, (d) Discharge capacity of VRFBs as functions of cycle number over 100 cycles.

The average VEs of the batteries for P-GF, O-GF and R-GF are 75.7 %, 81.4 % and 83.1 %, respectively. Therefore, as shown in Fig. 9c, the cell using R-GF electrode has the highest energy efficiency (79.0 %), compared with that of O-GF (76.6 %) and P-GF (70.8 %). Fig. 9d shows capacity decay for different GFs over 100 charge/discharge cycles. The R-GF and P-GF have the highest and the lowest discharge capacity throughout the cycles. However, the capacity decay curves for different GFs are almost parallel. Since all of the cells have identical electrolyte and membrane except the

electrode, it can be speculated that the electrode material is not the key factor responsible for capacity decay.

As for VRFB systems, the rate capability is also very important. So the cell performance using the R-GF electrode at various current densities was evaluated in Fig. 10. With the increase of current density, the discharge capacities and energy efficiency gradually decrease. At a low current density (50 $mA \cdot cm^{-2}$), the discharge capacities of different GFs electrodes have little difference. However, the difference becomes more and more obvious with the increasing of current density. When the current density reaches 100 $mA \cdot cm^{-2}$, the discharge capacity of R-GF (22.5 $Ah \cdot L^{-1}$) is 12.0 % higher than that of O-GF (20.1 $Ah \cdot L^{-1}$), and the cell using P-GF cannot even work at same condition owing to the severe polarization [33]. When the current density was adjusted back to 50 $mA \cdot cm^{-2}$, the EE values of different GFs are basically restored to the originals, but the discharge capacity of P-GF is obviously decreased compared with those of O-GF and R-GF. According to the previous reports [9, 10, 24, 34], oxygen-containing functional groups have an electrocatalytic effect on the redox reaction of vanadium ions especially at high current densities, by reducing electrochemical polarization. Therefore, the R-GF with larger surface area and more oxygen-containing functional groups can enhance the comprehensive performance of the VRFBs, such as VE, EE, electrolyte utilization and discharge capability at high current densities.

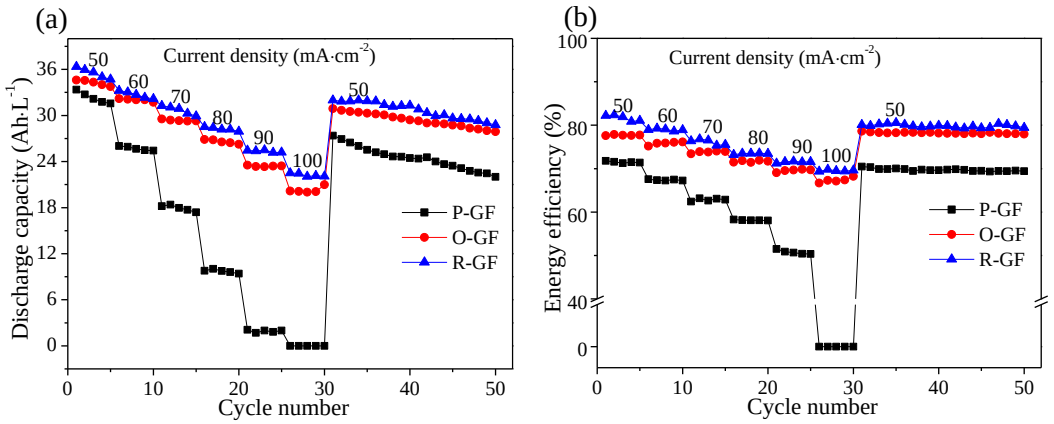

Figure 10. Electrochemical performance of VRFBs using P-GF, O-GF, and R-GF as electrodes: (a) Discharge capacity and (b) Energy efficiency of VRFBs with each type of GF as functions of cycle number at the current densities of 50-100 $mA \cdot cm^{-2}$.

Table 2 shows the comparison of results obtained in this work and those previously reported studies concerning to the etching modifications of carbon felts (CFs) and GFs. Due to the test conditions (carbon/graphite felts, electrolyte compositions, current densities, sizes and structures of the testing cells) are different, it is difficult to directly compare the results listed in the Table 2. However, considering the simplicity and cost-effectiveness, the method developed in this work has good application potential in the field of VRFB. In addition, the comparison of different methods for increasing GF surface area under the same testing conditions is being carried out, and the results will be reported in subsequent papers.

Table 2. The comparison of results obtained in this work and those previously reported.

Material	Method	electrode size (cm)	Electrolyte	Current density ($mA \cdot cm^{-2}$)	CE (%)	VE (%)	EE (%)	Ref.
GF	CO_2-activated (1000 °C)	5×5 [a]	1.6 M $VOSO_4$ /2.5 M H_2SO_4	50	94.5	90.1	84.1	[21]
GF	Water-activated (700 °C)	5×5×0.65	1.6 M $VOSO_4$ /2.5 M H_2SO_4	80	96.3	81.1	78.1	[22]
GF	etched by KOH (800 °C)	5×5×0.5	2 M $VOSO_4$ /2 M H_2SO_4	50	92.5	89.0	82.5	[23]
GF	etched by NiO (500 °C)	4×4×0.3	2 M $VOSO_4$ /5 M H_2SO_4	150	97.0	72.8	71.0	[24]
GF	etched by FeOOH (900 °C)	5×5×0.5	1.5 M $VOSO_4$ /2 M H_2SO_4	150	95.0	77.0	74.0	[25]
CF	etched by Co_3O_4 (400 °C)	5×5 [a]	1.5 M $VOSO_4$ /3 M H_2SO_4	50	96.8	89.9	87.3	[26]
GF	etched by Mn_3O_4	3×3×0.5	1.5 M $VOSO_4$ /3 M H_2SO_4	80	94.7	83.8	79.5	This work

a. Thickness not specified.

4. CONCLUSIONS

In this study, roughened GF has been successively prepared by a simple and cost-effective method using cheap manganese oxide (Mn_3O_4) as etching agent. The precursor concentration and the operating temperature of Mn_3O_4 reduction reaction are the critical factors in determining the roughness of R-GF. The R-GF prepared under the optimized conditions has the best electrochemical activity and kinetic reversibility compared with P-GF and O-GF. The VRFB using R-GF electrodes has high EE and utilization rate of electrolyte at different current densities, thus confirming the beneficial effects of the larger surface area with abundant oxygen-containing functional groups as catalytic centers. Therefore, this study provides a feasible approach to develop the GF electrode with high specific surface area which could be suitable for high-performance VRFB applications.

ACKNOWLEDGEMENTS
This work was partially supported by the National Key Research and Development Program of China (Project No. 2017YFB0307503).

References

1. B. Dunn, H. Kamath, J.M. Tarascon, *Science*, 334 (2011) 928.
2. W.J. Lu, X.F. Li, H.M. Zhang, *Phys. Chem. Chem. Phys.*, 20 (2018) 23.
3. K.J. Kim, M.S. Park, Y.J. Kim, J.H. Kim, S.X. Dou, M. Skyllas-Kazacos, *J. Mater. Chem. A*, 3 (2015) 16913.
4. M. Ulaganathan, V. Aravindan, Q. Yan, S. Madhavi, M. Skyllas-Kazacos, T.M. Lim, *Adv. Mater. Interfaces*, 3 (2015) 1500309.
5. M. Skyllas-Kazacos, M.H. Charkarbarti, S.A. Hajimolana, F.S. Mjalli, M. Saleem, *J. Electrochem. Soc.*, 158 (2011) R55.
6. M.H. Chakrabarti, N.P. Brandon, S.A. Hajimolana, F. Tariq, V. Yufit, M.A. Hashim, C.T. Low, P.V. Aravind, *J. Power Source*s, 253 (2014) 150.
7. Z.X. He, Y.Q. Jiang, W. Meng, Appl. Surface Sci., 423 (2017) 111.
8. K.J. Kim, S.W. Lee, T. Yim, J.G. Kim, J.W. Choi, J.H. Kim, M.S. Park, Y.J. Kim, *Sci. Rep.*, 4 (2014) 6906.
9. K.J. Kim, Y.J. Kim, J.H. Kim, M.S. Park, *Mater. Chem. Phys.*, 131 (2011) 547.
10. D.S. Yang, J.Y. Lee, S.W. Jo, S.J. Yoon, T.H. Kim, Y.T. Hong, *Int. J. Hydrogen Energy*, 43 (2018) 1516-1522.
11. Q. Deng, P. Huang, W. Zhou, Q. Ma, N. Zhou, H. Xie, W. Ling, X. Wu, X. Lu, Y. Guo, *Adv. Energy Mater.*, 7 (2017) 1700461.
12. B. Li, M. Gu, Z.M. Nie, Y. Shao, Q. Luo, X. Wei, X. Li, J. Xiao, C. Wang, V. Sprenkle, W. Wang, *Nano Lett.*, 13 (2013) 1330.
13. T.M. Tseng, R.H. Huang, C.Y. Huang, K.L. Hsueh, F.S. Shieu, *J. Electrochem. Soc.*, 160 (2013) A690.
14. L. Wei, T.S. Zhao, L. Zeng, X.L. Zhou, Y.K. Zeng, *Appl. Energy*, 180 (2016) 386.
15. D.M. Kabtamu, J.Y. Chen, Y.U. Chang, C.H. Wang, *J. Mater. Chem. A*, 4 (2016) 11472.
16. H. Zhou, Y. Shen, J.Y. Xi, X.P. Qiu, L.Q. Chen, *ACS Appl. Mater. Interfaces*, 8 (2016) 15369.
17. B. Li, M. Gu, Z.M. Nie, X.L. Wei, C.M. Wang, V. Sprenkle, W. Wang, *Nano Lett.*, 14 (2014) 158.
18. F.M. Zhao, G. Wen, L.Y. Kong, Y.Q. Chu, C.A. Ma, *Acta Phys. -Chim. Sin.*, 33 (2017) 1181.
19. F.M. Zhao, G. Wen, L.Y. Kong, Y.Q. Chu, C.A. Ma, *Chinese J. Inorg. Chem.*, 33 (2017) 501.
20. Y. Shao, Y. Cheng, W. Duan, W. Wang, Y. Lin, Y. Wang, J. Liu, *ACS Catal.*, 5 (2015) 7288.
21. Y.C. Chang, J.Y. Chen, D.M. Kabtamu, G.Y. Lin, N.Y. Hsu, Y.S. Chou, H.J. Wei, C.H. Wang, *J. Power Sources*, 364 (2017) 1.
22. D.M. Kabtamu, J. Chen, Y. Chang, C. Wang, *J. Power Sources*, 341 (2017) 270.
23. Z. Zhang, J.Y. Xi, H. Zhou, X.P. Qiu, *Electrochim. Acta*, 218 (2016) 15.
24. J.J. Park, J.H. Park , O. Park, J.H. Yang, *Carbon*, 110 (2016) 17.
25. Y.C. Liu, Y. Shen, L.H. Yu, L. Liu, F. Liang, X.P. Qiu, J.Y. Xi, *Nano Energy*, 43 (2018) 55.
26. S. Abbas, H. Lee, J. Hwang, A. Mehmood, H. Shin, S. Mehboob, J.Y. Lee, H.Y. Ha, *Carbon*, 128 (2018) 31.
27. N. Pour, D.G. Kwabi, T. Carney, R.M. Darling, M.L. Perry, Y.S. Horn, *J. Phys. Chem. C*, 119 (2015) 5311.
28. B. Jiang, L.H. Yu, L.T. Wu, D. Mu, L. Liu, J.Y. Xi, X.P. Qiu, *ACS Appl. Mater. Interfaces*, 8 (2016) 12228.
29. Y.F. Cheng, Z. Wei, Q. Du, F. Liu, X. Duan, Y. Wang, D.C. Jia, Y. Zhou, B. Li, *Electrochim. Acta*, 284 (2018) 408.
30. D. Qiu, N. Guo, A. Gao, R. Yang, *Electrochim. Acta*, 294 (2018) 398.
31. Z. González, C. Flox, C. Blanco, M. Granda, J.R. Morante, R. Menéndez, *J. Power Sources*, 338 (2017) 155.
32. G. Oriji, Y. Katayama, T. Miura, *J. Power Sources*, 139 (2005) 321.
33. S. Mehboob, G. Ali, H.J. Shin, J. Hwang, S. Abbas, K.Y. Chung, H.Y. Ha, *Appl. Energy*, 229

(2018) 910.
34. N. Pour, D.G. Kwabi, T. Carney, R.M. Darling, M.L. Perry, Y. Shao-Horn, *J. Phys. Chem. C*, 119 (2015) 5311.